Colloids and Surfaces A 534 (2017) 16–25

Contents lists available at ScienceDirect

Colloids and Surfaces A

journal homepage: www.elsevier.com/locate/colsurfa

Role of surface properties for the kinetics of bubble Ostwald ripening in saponin-stabilized foams

Slavka Tcholakova[a,*], Fatmegul Mustan[a], Nevena Pagureva[a], Konstantin Golemanov[b], Nikolai D. Denkov[a], Edward G. Pelan[b], Simeon D. Stoyanov[b,c,d]

[a] Department of Chemical and Pharmaceutical Engineering, Faculty of Chemistry and Pharmacy, Sofia University, 1J. Bourchier Ave., 1164 Sofia, Bulgaria
[b] Unilever R & D, Vlaardingen, The Netherlands
[c] Laboratory of Physical Chemistry and Colloid Science, Wageningen University, 6703 HB Wageningen, The Netherlands
[d] Department of Mechanical Engineering, University College London, Torrington Place, London WC1E 7JE, UK

GRAPHICAL ABSTRACT

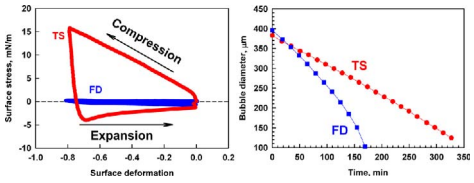

ARTICLE INFO

Keywords:
Foam coarsening
Ostwald ripening
Saponin
Adsorption layer
Surface rheology

ABSTRACT

Bubble Ostwald ripening (OR) leads to a gradual increase of the mean bubble size in foams with time. The rate of OR can be reduced significantly or even arrested completely using appropriate solid particles and/or surfactants as foam stabilizers. In the current paper, we show that saponins, a widespread class of natural surfactants, can reduce significantly the rate of OR in foams. To reveal the reasons for the reduced rate of OR in saponin-stabilized foams, we performed measurements of the rate of bubble diminishing, for single air bubbles placed below a solution surface, with a series of saponin bio-surfactants. These saponin surfactants form adsorption layers with surface elasticity, spanning a very wide range – from almost zero up to several thousand mN/m. The measured rate of bubble OR showed no correlation with the surface elastic modulus (dilatational or shear), as measured at 0.1 Hz frequency of surface oscillations. A reasonable correlation was observed only with the surface stress (deviation from the equilibrium surface tension), measured at very slow rate of surface deformation, which mimics much better the actual processes of bubble OR in foams – higher surface stress corresponds to lower OR rate. New theoretical expression, accounting for the out-of- equilibrium surface tension during bubble shrinkage and for the gas flux across the meniscus regions surrounding the foam films, was derived and used to calculate theoretically the rate of bubble diminishing. The comparison of the theoretical predictions with the experimental data shows clearly that the main reason for the reduced rate of OR in the studied systems is the high resistance to gas transfer of the saponin adsorption layers. The deviations from the equilibrium surface tension, although noticeable, have smaller effect. The complementary experiments with actual foams showed that the rate of OR is even lower (compared to the rate measured with single bubbles) which is explained with the thicker non-equilibrium foam films, formed between the neighboring bubbles in saponin-stabilized foams.

* Corresponding author.
E-mail address: sc@lcpe.uni-sofia.bg (S. Tcholakova).

http://dx.doi.org/10.1016/j.colsurfa.2017.04.055
Received 27 November 2016; Received in revised form 16 March 2017; Accepted 24 April 2017
Available online 29 April 2017
0927-7757/ © 2017 Elsevier B.V. All rights reserved.

1. Introduction

Foams encountered in practice usually contain bubbles with various sizes, in which the chemical potential of the gas molecules is different. This difference causes a molecular gas transport from the smaller bubbles toward the bigger ones. As a result, the mean bubble size in foams gradually increases and the related foam properties change with time. This process is usually called “foam coarsening” or “bubble Ostwald ripening” (OR). To emphasize that we are interested only in the molecular gas transfer across the foam films formed between neighboring bubbles and do not consider the effect of bubble–bubble coalescence, which may also contribute to the increase of bubble size in real foams (if coalescence occurs), we use hereafter only the term “bubble OR” for the processes studied in this paper.

The bubble size is an important parameter which affects the foam stability and the rate of water drainage [1–4], as well as the rheological [5–8], optical and many other foam properties. Therefore, it is of high practical and research interest to control the bubble OR in foams. There are several ways to decrease the rate of OR: (1) To use a gas with low solubility in water [3]; (2) To modify the bulk properties of the continuous phase. For instance, if the continuous phase has higher viscosity, the gas diffusion coefficient is lower and the rate of molecular transport is reduced accordingly [9,10]. (3) To stabilize the foam with solid particles; some particles are known to form a rigid shell on the bubble surface and to decrease or even to arrest completely the process of OR [11–14]; (4) To use appropriate surfactants, proteins, or surfactant mixtures which form an adsorption layer with low gas permeability and/or high surface elasticity [3,15,16]. (5) To trap species in the bubbles, which are insoluble in the continuous phase (e.g., insoluble gas) [17,18].

The first three options involve significant modifications of the foaming system or require foam stabilization by solid particles, which is not always possible. An alternative approach, widely used in practice, is to use appropriate surfactant systems acting simultaneously as efficient foaming agents and as inhibitors of bubble OR [3,15,16]. It was demonstrated already that surfactants forming condensed adsorption layers, characterized with high surface modulus and low gas permeability, could significantly reduce the rate of OR in foams [15].

An important class of natural surfactants of this type are the so-called “saponins”, found in various plant species [19–21]. The saponin molecules consist of a hydrophobic scaffold, called aglycone, and one or several hydrophilic oligosaccharide chains, connected via glycoside bonds to the aglycone. Many saponins are known to have high surface activity, non- trivial rheological properties of their adsorption layers [22–27], and pronounced biological activity [19,21,28–35], including anti-fungal, anti-bacterial, anti-inflammatory [30], anti- yeast [31,32], cholesterol-lowering [33–35], and anti-oxidant (potentially useful) effects. Therefore, various saponin extracts are already used as active ingredients in various pharmaceutical and food technologies. Still, the relation between the specific types of saponin, used as foaming agents, and the kinetics of bubble OR in foams has not been studied yet.

A study of this kind is important in another aspect as well. Two conceptually different explanations are proposed in the literature to explain the suppressed bubble OR in foams – one explanation stresses on the role of the high surface elasticity of the adsorption layers of surfactants or particles [11,13,14], whereas the second explanation is based on the fact that the condensed surfactant adsorption layers possess high resistance to the transfer of gas molecules. The first explanation seems to be relevant for particle stabilized foams, whereas the second explanation was found operative in some surfactant systems, where condensed adsorption layers were formed in the presence of long-chain fatty acids or fatty alcohols as co-surfactants [15].

The surface moduli of the series of saponin samples studied in the current paper, were measured to vary in a wide range [24–27] which allows us to use these systems for a systematic study of the effects of surface elasticity and gas permeability of the adsorption layers on the rate of bubble OR.

To quantify precisely the rate of bubble OR, we observed optically the rate of shrinkage of single bubbles, placed in saponin solutions, just below the respective solution–air interface. We analyzed theoretically the gas flux across the foam film, formed at the contact of the bubble with the solution surface, and across the meniscus region surrounding this foam film, accounting also for the possible decrease of the bubble surface tension in the process of bubble shrinkage. From the best theoretical fits to the experimental data we determined the gas permeability of the adsorption layers of the various saponins. These results are used to search for a correlation between the rate of bubble OR and the various surface properties. In addition, we measured the evolution of the bubble size distribution in real foams, stabilized with the same saponin extracts. The latter results were described by the theoretical model, developed in our previous article [15] and compared with the results, obtained with single bubbles.

2. Materials and methods

2.1. Materials

Table S1 in Supporting information provides information about the saponins studied: name abbreviations used in the text, suppliers, concentration of saponin molecules in each extract, part of the plant which was processed for saponin extraction. For more detailed information, see Table 1 and Figure 1 in Ref. [25]. It is important to note that only one of the studied saponins is a pure chemical substance: Escin type II, molecular formula $C_{54}H_{84}O_{23}$, product of Sigma, cat. numb. 50531, CAS Number 6805-41-0. The other samples are non-purified plant extracts, containing a mixture of chemical compounds such as polyphenols, phenolic acids and polysaccharides [36]. Given extract typically contains a range of different saponins which share the same type of aglycone and differ in their hydrophilic oligosaccharide chains. Thus HC denotes an extract from Horse Chestnut (*Aesculus hippocastanum*) which contains Escin as a main saponin component. The majority of the studied saponins have triterpenoid aglycone from the oleanane type. Only the extract from *Yucca Schidigera* contains steroid saponins. Figure S1 in supporting information presents the basic molecular structures of the saponins studied.

The experiments were performed with solutions containing 0.5 wt% saponins and 10 mM NaCl. This high saponin concentration was used to ensure stable foams and bubbles with respect to coalescence, in the course of the experiments. It is more than 5 times higher than the critical micelle concentrations (CMC) of all saponins studied. Table S2 provides information on the properties of the saponin solutions: CMC, pH, concentration of Ca^{2+}, viscosity, equilibrium surface tension and equilibrium film thickness, as determined in experiments with single foam films in capillary cell [37].

2.2. Methods

2.2.1. Foam formation and evolution of the mean bubble size

The initial foam, containing bubbles with diameter of 0.1 to 0.2 mm, was prepared by a series of ejection/injection cycles of the foaming solution through a syringe needle [38]. This foam was introduced into a petri dish with height of 3 mm (to avoid significant water drainage in the foam) and covered by an optical prism to avoid evaporation and gas diffusion across the foam/atmosphere interface. The petri dish was placed in a thermostatted chamber and the temperature was maintained at 20 ± 0.2 °C during the experiment.

The bubble size distribution in the foam was determined by using the procedure developed by Garrett et al. [15,39]. A video camera, equipped with long-working-distance magnifying lens, was focused on a certain region in the foam sample which was in contact with the glass prism, and used to capture images of the bubbles for a period of 1 h, see Figure S2. The bubble size distribution was determined from these

images by using the relation $R_B = (A_{BP}/\pi)^{1/2}$, where A_{BP} is the projected area of a given bubble in contact with the prism wall. Image analysis software is used to determine the distribution of the projected bubble areas on the prism wall and, hence, of the bubble size distribution in a given moment of the experiment. In this way, we were able to record the evolution of bubble size distribution, as a function of the coarsening time, t. It is known from literature that the bubble size distribution near the walls of the foam container is not exactly the same as in the bulk foam. However, as shown by Wang & Neethling [40] the difference between the size distributions, determined from the 2D film size distribution and the actual 3D bubble size distribution, decreases with the increase of bubble polydispersity. As far as our foams are rather polydisperse, we do not expect a significant difference between the measured bubble size distribution near the solid glass wall and the actual bubble size distribution inside the bulk foam.

We checked carefully the video-records of all samples for possible bubble coalescence during the experiment. All systems discussed here did not exhibit any bubble–bubble coalescence during the entire observation period. From the experimental data for the bubble size evolution in bulk foams, we determined the gas permeability by using the theoretical model developed in a previous study [15]. This model is an upgrade of the model by Lemlich [41] who employed Fick's law to account for the molecular gas transfer between dispersed bubbles and to derive an expression for the evolution of the bubble size in bubbly liquids (separate bubbles, not touching each other). The gas chemical potential and the related rate of bubble size evolution are calculated from the gas pressures in the bubbles of various size, under the assumption that the gas is ideal:

$$\frac{dR_i}{dt} = -\frac{2\sigma K_L}{p_0}\left(\frac{1}{R_i} - \frac{1}{R_{21}}\right) \quad (1)$$

Here p_0 is the atmospheric pressure, σ is the surface tension, K_L is the total permeability across the surface of the bubbles (toward the liquid medium) for the gas molecules, and R_{21} is the mean surface-length bubble size (see Refs. [15,41] for its definition). The gas permeability across a foam film, with an account of the possible effect of the surfactant adsorption layers, was defined in a separate study by Princen and Mason [42]:

$$K = \frac{DH}{h + 2D/k_{ML}} \quad (2)$$

Here h is the foam film thickness (more precisely, of the aqueous interior of the foam film), k_{ML} is the gas permeability of the individual adsorption layers on each of the film surfaces, D is the diffusion coefficient of the gas in the liquid medium, H is the Henry's constant for the gas solubility in the same liquid medium. The ideas of Lemlich [41] and Princen and Mason [42] were combined and further elaborated in Ref. [15] to account for the effect of air volume fraction in the actual foams on the kinetics of bubble size evolution. The effect of the air volume fraction in the foam on the size of the formed foam films and on the pressure inside the bubbles was explicitly taken into account and a set of differential equations to describe the bubble size evolution was derived and solved numerically [15].

The main equations of the model developed in Ref. [15] are briefly introduced below, as they are used to interpret the data from the experiments with actual foams in the current study. The air volume fraction, Φ, in the studied foams is above the value for close packing of spherical bubbles, Φ_{CP}. Therefore, the bubbles deform to form polyhedrons with foam films between them. The change of the size of bubbles with radius R_i over time is presented via the expression [15]:

$$\frac{dR_i}{dt} = -F(\Phi)\left(\frac{1}{R_i} - \frac{1}{R_{21}}\right) \quad (3)$$

where $F(\Phi)$ is a function of the air volume fraction and the material characteristics of the foam only, and it does not depend on the bubble size and time [15]:

$$F(\Phi) = K\frac{S_F}{S_0}\frac{\sigma}{p_0}\left(\frac{1-\Phi}{\Phi}\widetilde{P}_{OSM}(\Phi) + 2\frac{S(\Phi)}{S_0}\right) \quad (4)$$

Here S_F is the total area of the foam films, S is the total area of the deformed bubbles, S_0 is the total area of the non- deformed bubbles, and $\widetilde{P}_{OSM}$ is the dimensionless osmotic pressure in the foam (the ratios S_F/S_0 and S/S_0 depend on Φ only). Eq. (3) shows that, in any given moment, the bubbles with size bigger than R_{21} will grow, while those with size smaller than R_{21} will diminish, as a result of the Ostwald ripening process. We employ a numerical procedure [15] to predict theoretically the evolution of the bubble size distribution, and from the best fit to the respective experimental data we can determine the only adjustable parameter in the model, namely the gas permeability across the foam films, K. From the values of K and Eq. (2) one could determine the permeability of the surfactant adsorption layers, k_{ML}, once the values of the other parameters, D, H and h are determined.

2.2.2. Evolution of the size of a single bubble under solution–air interface

By this method, we determined the gas permeability for a foam film, formed between a single bubble and large air–water interface (the bubble is attached to the interface by gravity) [15,43–46]. A single bubble with an initial radius of around 200 μm was placed below the surface of a saponin solution, in a petri dish mounted in a thermostating cell. The experiments were performed at constant temperature of 20 °C. The radius of the bubble was measured in transmitted light with optical microscope (Axioplan, Zeiss, Germany). We observed also in reflected light the foam film, formed between the bubble and the solution surface. The pressure in the bubble is higher than the atmospheric pressure, which causes a gas flux across the foam film toward the atmosphere – as a result, a gradual decrease of the bubble size with time is observed. The changes in the bubble and film radii were recorded over a period of several hours. The kinetics of this process can be analyzed to yield the foam film permeability, K.

2.2.3. Rheological properties of saponin adsorption layers under slow deformation

The rheological properties of saponin adsorption layers were studied in Refs. [24–27] using several methods, which were applied at different frequencies, amplitudes and modes of deformation (dilatational and shear). Here we describe only the Langmuir trough method which allows very slow surface compression and expansion with large amplitude, thus, mimicking closely the dynamics of the adsorption layers on the surface of slowly shrinking or expanding bubbles. We used a Langmuir trough, model 302LL/D1 of Nima Technology Ltd., UK. The area of the trough was varied with two parallel barriers which moved symmetrically at a predefined linear speed. The surface pressure was measured with a Wilhelmy plate made of chromatographic paper. The plate was positioned in the middle between the barriers and oriented parallel to the barriers, see Figure S3 in supporting information. The layers were subjected to steady deformation in compression and expansion. The layers were deformed for ≈1500 seconds with a minimal possible speed of 0.0001 s^{-1} up to deformation ≈70%. The following experimental protocol was used: (1) Open the barriers to the maximum possible area (200 cm^2); (2) Wait until the equilibrium surface tension is reached; (3) Begin slow compression of the layer with a constant speed of the barriers at 0.083 cm^2/s down to surface area of 95 cm^2; (4) Start expanding the layer back to 200 cm^2 surface area. The surface stress is negative on expansion (σ higher than the equilibrium value) and positive on compression (σ lower than the equilibrium value). All experiments in Langmuir trough were performed at room temperature (≈23 ± 3 °C).

3. Results and discussion

First, we present and discuss the results, obtained in experiments with single bubbles. This method for determining the gas permeability, K, as described in Section 2.2.2, has the advantage of using less assumptions and approximations than the method of bubble size evolution in actual foams (Section 2.2.1). Therefore, we use the single bubbles as the main method for determination of K, whereas the measurements with actual foams are used for comparison and for further discussion of some of the obtained results.

3.1. Model experiments with single bubbles under air–water interface

We used saponin solutions with concentration of 0.5 wt%, at natural pH of the extracts, containing 10 mM NaCl. For each saponin we measured the change in the radius of at least 3 bubbles in separate experiments. The experimental results for the evolution of bubbles with similar initial radius, $R_0 \approx 200$ μm, are compared in Figure S4 in supporting information. The slowest change in R is observed for bubbles in solutions of Escin and TS, while the bubbles in solutions of SAP and FD disappear with the highest rate.

To determine the gas permeability of the respective foam films and saponin adsorption layers, we have to define precisely the region across which the main gas flux occurs. In Ref. [15] we used successfully a simple theoretical expression for the rate of bubble diminishing, derived under the assumption that the gas is transported across the foam film only and we have neglected the gas transport through the meniscus region. The film radius was determined from the balance of gravitational and capillary forces, under the assumptions that the contact angle between the film and the surrounding meniscus region is close to zero, and the bubble is slightly deformed (small Bond number). These assumptions led [15] to the following simple expression for description of the experimental data:

$$K_{\text{bubble}} = -\frac{3P_{\text{atm}}}{2\Delta\rho g t}\ln\frac{R_{\text{B}}(t)}{R_{\text{B}}(t=0)} \tag{5}$$

Here K_{bubble} is the permeability of the foam film, as determined from the experiments with single bubbles, P_{atm} is the atmospheric pressure, $\Delta\rho$ is the mass density difference between the liquid and gas phases, g is the gravity acceleration, $R_{\text{B}}(t)$ is the size of the bubble after a given period of time, t, and R_{B} ($t = 0$) is the initial bubble radius. According to Eq. (5), the logarithm of the decreasing bubble radius should be a linear function of time, with slope proportional to the film permeability.

To test whether Eq. (5) describes accurately the behavior of the saponin-stabilizied bubbles, we plotted the experimental data as ln [$R_{\text{B}}(t)$] vs. t, see Figure S5 in Supporting information. One sees that Eq. (5) describes well the size of the diminishing bubbles only until the bubbles reach a radius of ≈150 μm. When the bubble radius becomes smaller than ca. 150 μm, the bubbles in all systems shrink faster than the theoretical prediction by Eq. (5), see Figure S5. This deviation from the simplest theoretical model, Eq. (5), is explained by the noticeable contribution of the additional gas flux across the meniscus region surrounding the foam film, which is not accounted for in Eq. (5), and which cannot be neglected for the smallest single bubbles. The next section is dedicated to a theoretical analysis of the gas flux across the meniscus region.

3.2. Analysis of the gas flux across the meniscus region around the foam films

In the analysis below we assume that the gas flux occurs across two regions: (1) Foam film, which has constant thickness, h_0; (2) Meniscus region surrounding the foam film, in which the thickness of the liquid layer, $h(r)$, gradually increases with the distance from the film center, see Figure S6. Therefore, the total gas flux can be presented by the expression:

$$\frac{dn}{dt} = -\frac{2\pi\Delta p}{\mathbf{R}T}\left[\int_0^{R_F} K(h_0)rdr + \int_{R_F}^{R_B} K(r)rdr\right] \tag{6}$$

Here n denotes the moles of gas inside the bubble (i.e. dn denotes the moles transported from the bubble into the atmosphere, as a result of the bubble Ostwald ripening), Δp is the difference between the pressure inside the bubble and the atmospheric pressure, $\mathbf{R}$ is the universal gas constant, T is temperature. The first and the second integrals account for the gas flux across the foam film and across the meniscus region, respectively. R_F and R_{B} are the radii of the film and of the bubble, and $K(r)$ is the local gas permeability which is expressed by an upgrade of Eq. (2) and includes the permeability of the surfactant adsorption layer, k_{ML}:

$$K(r) = \frac{DH}{h(r) + 2D/k_{\text{ML}}} \tag{7}$$

To account for the gas flux across the meniscus region we need an expression for the variation of the layer thickness with the radial coordinate, r. Figure S6 presents schematically a bubble, placed under a flat air–water interface. For simplicity, we assume hereafter that the bubble surface is a part of sphere, i.e. the bubble is only slightly deformed by gravity (small Bond number). Indeed, the bubbles studied here have $R_{\text{B}} < 200$ μm and the respective bond number is $Bo < 0.013$. This additional assumption allows us to use the following expression for the thickness of the liquid layer:

$$h(r) = h_0 \quad 0 \le r \le R_F \tag{8}$$

$$h(r) = h_0 + R_B - \sqrt{R_B^2 - (r - R_F)^2} \quad R_F \le r \le R_B \tag{9}$$

Eq. (8) shows that the thickness of the planar film with radius R_{F} has constant thickness h_0. Eq. (9) implies that the thickness of the liquid layer around the film, in the surrounding meniscus region, is determined by the curved bubble surface (with radius of curvature R_{B}) which meets the film periphery with zero contact angle film-meniscus at $r = R_{\text{F}}$ (see Eq. (9) and Figure S6).

As in Ref. [15], we determine the film radius from the balance of the gravitational and capillary forces:

$$R_{\text{F}}^2 = \frac{4\Delta\rho g}{3\sigma}R_{\text{B}}^4 \tag{10}$$

Here σ is the surface tension. This expression is strictly valid for films with contact angle film-meniscus equal to zero [47] . After we substitute the expression for $h(r)$ from Eq. (8) into the expression for $K(r)$, the first integral in Eq. (6), related to the gas flux across the foam films, can be expressed explicitly as follows:

$$\int_0^{R_{\text{F}}} K(h_0)rdr = \int_0^{R_{\text{F}}} \frac{\text{DH}}{h_0 + 2D/k_{\text{ML}}}rdr = \int_0^{R_F} \frac{DH}{h_1}rdr = \frac{\text{DH}}{h_1}\frac{R_{\text{F}}^2}{2} = K_{\text{bubble}}\frac{R_{\text{F}}^2}{2} \tag{11}$$

Here $h_1 = h_0 + 2D/k_{\text{ML}}$ is a fictional thickness of a foam film which would have the same gas permeability as the real foam film, however, at negligible gas resistance of the surfactant monolayers. The difference between the value of h_1 and the actual thickness of the foam film, h_0, brings information about the relative contribution of k_{ML} into the total gas permeability of the foam films.

The second integral in Eq. (6), related to the gas flux across the meniscus region, can be expressed as:

$$\int_{R_{\text{F}}}^{R_{\text{B}}} K(r)rdr = \int_{R_{\text{F}}}^{R_{\text{B}}} \frac{\text{DH}}{h_1 + R_{\text{B}} - \sqrt{R_{\text{B}}^2 - (r - R_{\text{F}})^2}}rdr = I(R_{\text{B}}) \tag{12}$$

The integral in Eq. (12) was solved numerically and the total gas flux was presented in Eq. (6) as follows:

$$\frac{dn}{dt} = -\frac{2\pi\Delta p}{\mathbf{R}T}\left[\frac{\mathrm{DH}}{h_1}\frac{R_\mathrm{F}^2}{2} + I(R_\mathrm{B})\right] \quad (13)$$

After substituting the expression for the change of the moles of gas (see Eq. (S1) in Supporting information) in Eq. (13) and taking into account that the pressure difference between the bubble and the atmosphere is $2\sigma/R_\mathrm{b}$ one obtains:

$$\frac{p_0}{\mathbf{R}T}4\pi R_\mathrm{B}^2\frac{dR_\mathrm{B}}{dt} = -\frac{4\pi\sigma}{\mathbf{R}TR_\mathrm{B}}\left[\frac{\mathrm{DH}}{h_1}\frac{R_\mathrm{F}^2}{2} + I(R_\mathrm{B})\right] \quad (14)$$

After introducing the expression for the film radius into the above equation, we obtain the following expression for the change in the bubble radius with time:

$$\int_{R_\mathrm{B}}^{R_\mathrm{B0}}\frac{1}{Y(R_\mathrm{B})}dR_\mathrm{B} = \frac{2}{3}\int_0^t\frac{DH\Delta\rho g}{h_1p_0}dt = \frac{2}{3}\frac{DH\Delta\rho g}{h_1p_0}t = \frac{2}{3}K_\mathrm{bubble}\frac{\Delta\rho g}{p_0}t \quad (15)$$

where

$$Y(R_\mathrm{B}) = R_\mathrm{B}\left[1 + \frac{2h_1}{R_\mathrm{F}^2}\int_{R_\mathrm{F}}^{R_\mathrm{B}}\frac{r}{h_1 + R_\mathrm{B} - \sqrt{R_\mathrm{B}^2 - (r - R_\mathrm{F})^2}}dr\right] \quad (16)$$

The integral in Eq. (16) was calculated numerically. From the best fit to the experimental data by Eqs. (15) and (16) we determined the value of K_bubble which accounts for the total gas flux across both the film and the meniscus regions. Thus we have formulated a complete set of equations needed to interpret the experimental data, obtained with single bubbles.

Fig. 1 compares the best fits of the experimental data for bubble size diminishing with time without accounting for gas flux through the meniscus region and with accounting for this contribution. The experimental data provide the dependence of the bubble radius on time. To determine the value of h_1 we solved numerically the transcendental equation, Eq. (15). The material parameters used to solve Eq. (15) are the surface tension, gas diffusion coefficient, Henry constant for gas solubility in water, mass density difference between air and surfactant solution, gravity constant and atmospheric pressure – their values are presented in Table S2 in Supporting information. We solve Eq. (15) for each experimental point and, thus, we determine a series of values of h_1. From these values we calculate the mean value of h_1 and its standard deviation. This procedure is applied for 4 independently determined data sets for FD stabilized bubbles, as shown in Fig. 1. The green theoretical curve in Fig. 1 is calculated under the assumption that h_1 is the same for all these bubbles during the entire observation period. One sees that the gas flux across the meniscus region is substantial even during the initial stages of the experiments with single bubbles. In other words, by neglecting the gas flux across the meniscus region we overestimate the gas permeability of the adsorption layers, as determined in the experiments with individual bubbles. Note that this conclusion is valid only for the experiments with single small bubbles, in which the foam films are formed only as a result of gravity and are, therefore, rather small in diameter (cf. Eq. (10)). The films between neighboring bubbles in actual foams with air volume fraction of ca. 90%, are several times bigger in diameter, as these films are formed between geometrically constrained bubbles. As a consequence the gas transfer through the meniscus region for bubbles in foams with volume fraction of 90% and above can be neglected, whereas at lower air volume fractions most probably it will affect the overall rate of foam coarsening.

The results for $K_\mathrm{bubble} = \mathrm{DH}/h_1$, which account explicitly for the contribution of the meniscus region, are presented in Fig. 2 for different saponins. One should be mentioned that the values of K_bubble, determined in different moments of the experiments with diminishing bubbles, were scattered around the mean value shown in Fig. 2 for Sapindin, FD, HC and QD samples. In contrast, a noticeable decrease of K_bubble with time was observed for Escin, TS and BSC (three saponin extracts with high surface elasticity) which indicates that significant changes in the structure of adsorption layers could take place for these saponins. These changes may lead to lower surface tension of the bubble, decreased permeability of the adsorption layers and/or other effects that reduce the rate of Ostwald ripening (see below for additional discussion of these effects). For example, the value of K_bubble for Escin decreased from 250 μm/s down to 55 μm/s in the course of the experiment. Therefore, in Fig. 2 we show the values of K_bubble for Escin, TS and BSC, which are averaged over the whole period of bubble diminishing, from 6 independent experiments. One sees that the mean values of K_bubble varied from ≈ 100 μm/s for Escin up to ≈ 680 μm/s for sapindin.

3.3. Relation between the gas permeability of the foam films and the rheological properties of the adsorption layers

There are two main contributions to K_bubble – one related to the gas flux across the aqueous interior of the foam film, and the other related to the gas flux across the adsorption layer, denoted as k_ML, see Eq. (7). To account for the gas flux across the liquid interior of the films, we measured the equilibrium thickness of the foam films, stabilized by different saponins, see Table S2 for the results. The dissolved saponins are in a very low concentration to affect significantly the gas solubility in the aqueous phase. Therefore, we used values for H and D known from literature for pure water with viscosity of 1 mPa s: $H \approx 0.0199$ [15], and $D \approx 2 \times 10^{-9}$ m^2/s [15,42]. To account for the increased viscosity of some of the studied saponin solutions, as a result of the saponin dissolution, we assumed that D is inversely proportional to the viscosity of the aqueous phase. The used values for the gas diffusion coefficients in the studied saponin solutions are shown in Table S2.

The effective film thickness, h_1 (accounting for the gas diffusion across both the liquid core and the adsorption layers) is calculated from the expression $h_1 = \mathrm{DH}/K_\mathrm{bubble}$. The comparison of h_1, calculated from the gas permeability of the foam films and the actual film thickness, h_0, as measured in a capillary cell, shows that the contribution of the adsorption layer to the overall film resistance is significant for all studied saponin solutions, see Fig. 3. The largest effective film thickness, corresponding to the lowest gas permeability across the adsorption layers, is determined with Escin (ESC) and tea saponin (TS) solutions. Highest permeability is determined with Sapindin (Sap), Horst Chestnut (HS) and Foamation Dry (FD, Yucca extract) saponin solutions. Intermediate effect is observed with Quillaya (QD) and Berry (BSC) saponin solutions.

Next we tried to find a correlation between the gas permeability across the adsorption layers of various saponins, k_ML, and the rheological properties of these layers. In Fig. 4 we present k_ML plotted vs. the

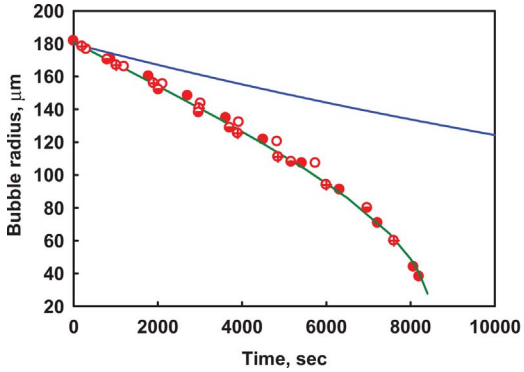

Fig. 1. Bubble radius as a function of the time, for bubbles (different symbols correspond to different bubbles in different experiments) in a solution of FD. The analysis accounts for the gas flux across the foam film only (blue curve) or for the flux across both the foam film and the meniscus region (green curve). (For interpretation of the references to colour in this figure legend, the reader is referred to the web version of this article.)

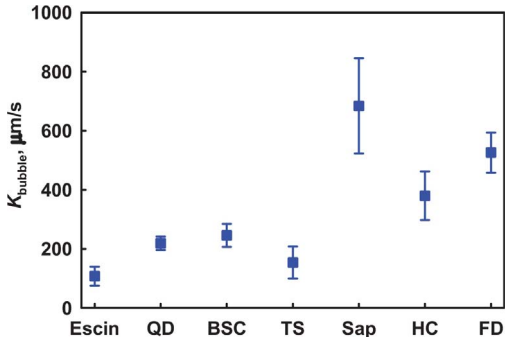

Fig. 2. Gas permeability of foam films between single bubble and a large air–water interface, for bubbles placed in solutions of different saponins. The results for K_{bubble} are obtained by fitting the experimental data for the evolution of the bubble radius by Eq. (15) which accounts for the gas flux across the meniscus region.

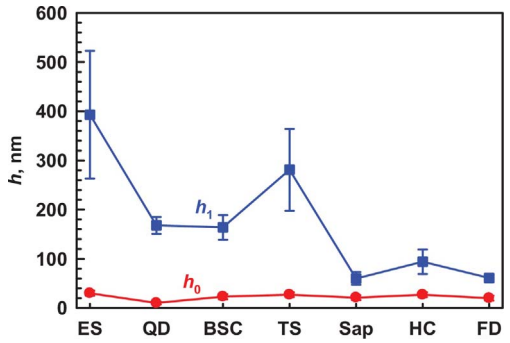

Fig. 3. Effective thickness of a liquid film for gas flux, h_1, determined from the experiments with a single bubble under air–water interface. Real thickness of the foam films, h_0, measured in a capillary cell from the intensity of the light reflected from the films [37].

dilatational and shear elasticities of the respective saponin layers. These elasticities were measured in Langmuir trough, at a frequency of oscillations of 0.1 Hz, as described in Ref. [27] . We determined $k_{ML} < 30$ mm/s for BSC, TS, QD and ESC, while for HC, FD and Sap the value of k_{ML} is between 50 and 100 mm/s. For comparison, ESC, QD, TS and BSC exhibited very high dilatational elasticity (> 100 mN/m) and relatively high shear elasticity (> 10 mN/m), whereas the dilatational elasticity was lower than 50 mN/m and the shear elasticity was practically zero for all other saponins. One sees from Fig. 4 that lower gas permeability of the adsorption layers is related to higher surface elasticity, however, this general trend is not observed as a clear correlation – the points do not fall around a single master curve.

As far as the dilatational and shear elasticities shown in Fig. 4 are determined at relatively high rate of surface deformation (compared to the rate of surface shrinking or expansion in the case of bubbles OR), for the current study we performed additional rheological experiments in which we expanded and contracted the saponin adsorption layers at the lowest possible speed of the barriers in the Langmuir trough. The experimental procedure is described in Section 2.2.3. Fig. 5A presents the results for the surface stress, as a function of surface deformation, realized in sequential compression and expansion cycles of the adsorption layer. The shear rate during these experiments varied between $5 \times 10^{-4}\,s^{-1}$ and $0.001\,s^{-1}$ (the velocity of the moving barriers was fixed). This deformation rate corresponds to a characteristic deformation time of the order of 1000 to 2000 seconds which is more representative for the slow processes of bubble shrinkage/expansion during Ostwald ripening, as compared to the typical oscillation type of experiments with bubbles and drops (with typical frequency of 0.1 to 1 Hz). The stress is defined as a difference between the equilibrium surface tension and the instantaneous surface tension during surface compression or expansion. The initial surface pressure is equal to the equilibrium surface pressure after adsorption of the saponin molecules on the air/water interface. The dynamic pressure isotherm is not symmetrical with respect to surface deformation because the kinetics of desorption of the molecules from the adsorption layer is significantly slower as compared to the rate of their adsorption. As a consequence, the measured surface tension during surface compression is much lower than the equilibrium one, whereas it is very close to the equilibrium one upon surface expansion. The negative surface stress in this case reflects the fact that the surface tension is slightly higher than the equilibrium one. The higher surface tension upon expansion is due to the fact that the surface relaxation is not completed in the time scale of this experiment.

As seen from Fig. 5A, there is a significant difference in the surface stress upon compression and expansion for QD, ES, TS (all saponins with very high surface elasticities), whereas this difference is negligible for FD (a saponin with low surface elasticity). For all systems studied, the surface stress during compression is larger in magnitude than the stress during expansion, at the same strain of deformation.

We determined the maximum stress between the compressed and expanded layers, $\Delta\sigma$, and the resulting values are used to plot in Fig. 5B the dependence of k_{ML} on $\Delta\sigma$ for the studied saponins. A reasonably good correlation is observed between the gas permeability across the adsorption layer and the surface stress of slowly compressed adsorption layers. This correlation is much better as compared to the correlation between k_{ML} and the dilatational elasticities, measured at 0.1 Hz oscillation frequency, as can be seen from Fig. S7 in Supporting information. This correlation indicates that in the analysis of the experiments with the single bubbles, we might need to take into account the possible decrease of the surface tension of the diminishing bubbles – this decrease of the surface tension would reduce the capillary pressure of the shrining bubbles (proportional to bubble surface tension) which is the driving force for the bubble Ostwald ripening.

To account for the possible decrease of bubble surface tension upon its shrinkage, we fitted the experimental data for σ vs. surface deformation from the Langmuir trough with a polynomial equation and used this equation to estimate the bubble surface tension in the process

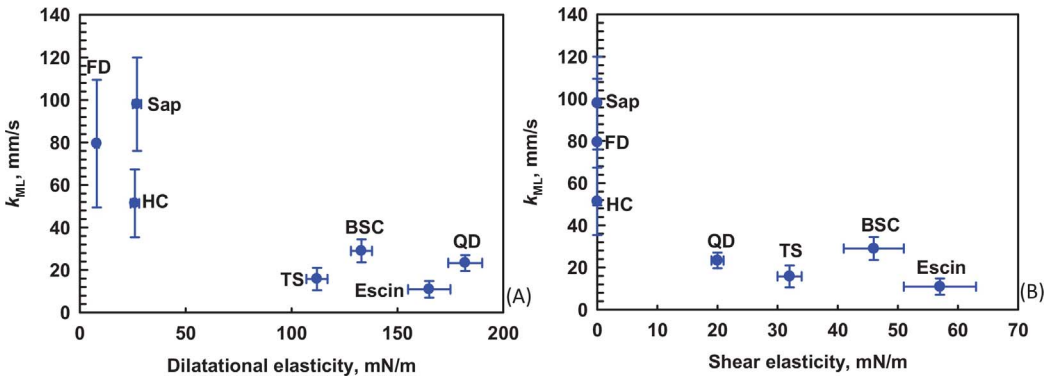

Fig. 4. Gas permeability of the adsorption layers of various saponins, plotted versus the surface elasticity of the adsorption layers, as measured at 5% amplitude of deformation and 0.1 Hz frequency of deformation in: (A) Dilatational deformation, (B) Shear deformation. The data for the surface elasticity are taken from Ref. [27].

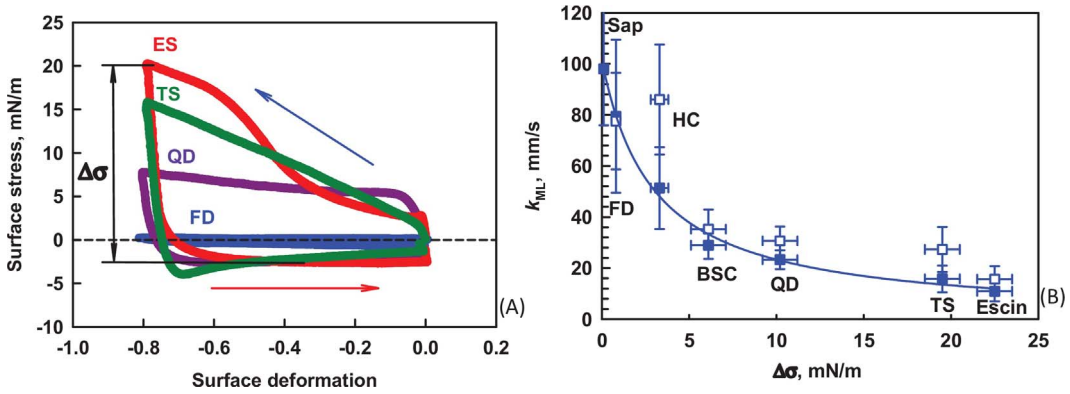

Fig. 5. (A) Surface stress of saponin adsorption layers under successive cycles of compression and expansion of the surface area for QD, ES, TS and FD saponin samples (the blue arrow shows the direction of surface compression, while the red arrow shows surface expansion). The experiments are performed with Wilhelmy plate which is oriented in parallel to the moving barriers and the shear rate is between 5×10^{-4} and 0.001 Hz, depending on the barriers position; (B) Correlation between the gas permeability across the adsorption layers and the maximum surface stress, measured as shown in (A). The full symbols show the values for k_{ML} determined assuming constant surface tension of the diminishing bubble. The empty symbols show the values of k_{ML} determined after accounting for the possible decrease of the bubble surface tension during its shrinkage. The surface stress is defined as a difference between the equilibrium and instantaneous surface tension during compression or expansion of the surface. (For interpretation of the references to colour in this figure legend, the reader is referred to the web version of this article.)

of bubble shrinkage. The accounted decrease of sigma with time leads to value of K_{bubble}, which does not depend significantly on time, see the pink points in Fig. 6. Nevertheless, the values of h_1 determined under the assumption for varying surface tension, remain much higher than h_0 which means that the gas permeability of the adsorption layers of ESC, TS, BSC and QD still remains much lower, as compared to that of HC, SAP and FD (see the empty points in Fig. 5B). Therefore, the main effect of the saponins on the rate of bubble Ostwald ripening is to reduce significantly the gas permeability of the adsorption layers on foam film surfaces, most probably, via formation of condensed saponin adsorption layers.

3.4. Kinetics of Ostwald ripening in foams formed from saponin solutions at natural pH

We were able to produce stable foams with Φ = 90% with all saponin extracts, described in Table S1. The results from the experiments with some other saponins (extracts of *Panax Ginseng*, *Tribulus Terrestris* or Fenusterols®), whose surface properties were studied in our previous articles [25,27], are not reported here, because we observed bubble–bubble coalescence during the experiments with these systems.

The change in the mean volume-surface bubble radius, R_{32}, with time in foams, stabilized by different saponins, is presented in Fig. 7. The rate of OR is the highest in the case of FD (steroid aglycone), and it is the slowest with ESC (triterpenoid aglycone).

The evolution of the bubbles in bulk foams was described with the theoretical model developed in Ref. [15], see the solid lines in Fig. 7. As seen from Fig. 7, the model describes very well not only the change of the mean volume-surface radius R_{32}, but also the change of the other mean sizes, and of the overall bubble size distributions as well, for most of the systems studied.

We determined the film permeability from foam experiments, K_{foam}, for the studied systems, from the best fits to the experimental data. We should note that we could not describe consistently the data for all mean radii with a single value of K_{foam} for some of the systems studied. Indeed, in the theoretical model [15] we assume that all bubbles have the same surface tension, while, as shown in the previous section, the shrinkage bubbles may have lower surface tension, as compared to expanding bubbles (which have almost equilibrium surface tension). Such systems are QD, TS, BSC, ESC, all of them characterized with rather high surface elasticity. This variation of σ, in turn, may affect the driving force of the OR process, as the capillary pressure in each bubble depends on its specific value of the surface tension (unless all bubbles have the equilibrium surface tension of the surfactant solution).

To perform a quantitative comparison of the different systems, we processed the foam data under the assumption that all bubbles have the same surface tension (the equilibrium one) and compared the results for K_{foam}, obtained from the best fit to the data for the mean radius R_{32}, see Fig. 8. One sees that the values of K_{foam} vary significantly, depending on the particular saponin extract stabilizing the foam. Fig. 8B compares the results for K_{bubble} and K_{foam} for the different saponins. We see that we have consistent results for TS and reasonable agreement for ES, however, the rate of bubble OR in bulk foams appears as significantly lower (compared to the rate of OR of single bubbles) for the other saponins, as characterized by the value of film permeability, K.

One difference between TS and Escin on one hand, and the rest of the saponins on the other hand, is that the saponin concentration in the TS and ES extracts is above 95 wt%, while the saponin content is lower in the other extracts, see Table S1. Therefore, a possible explanation for the observed difference between the results obtained with single bubbles and with bulk foams could be that the composition of the adsorption layers is different in these two types of experiments. Indeed, the hydrodynamic conditions in these experiments are rather different – for example, the bubble interfaces are subjected to multiple compression and expansion cycles during the foam generation with a syringe, which is not the case in the experiments with single bubbles. As a result of these cycles, surface active ingredients with low solubility might be transported to the bubble surface in bulk foams, pack there along with the main surface active components, and additionally hinder the gas

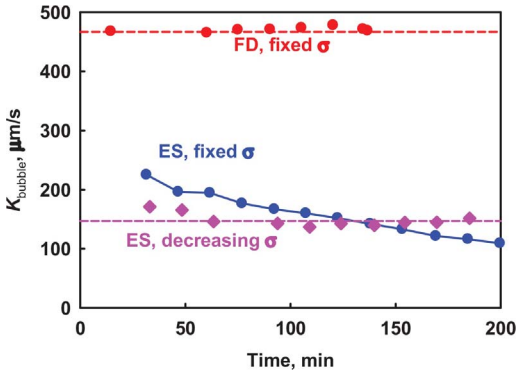

Fig. 6. Film permeability as a function of time for FD (red symbols) and Escin (blue circles), calculated under the assumption for constant surface tension during bubble shrinkage. Pink diamonds represent data for Escin, calculated using the surface tension measured in the Langmuir trough. (For interpretation of the references to colour in this figure legend, the reader is referred to the web version of this article.)

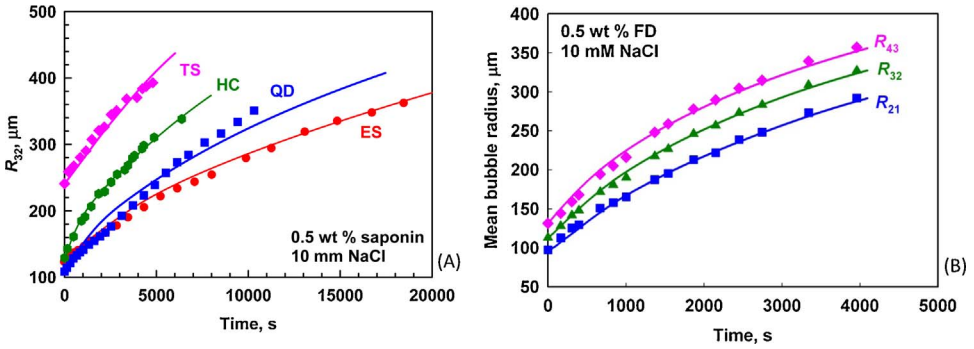

Fig. 7. (A) Evolution of the mean bubble size, R_{32}, in foams stabilized by different saponins as indicated in the figure. (B) Experimental data for the mean radii of the bubbles in foam, stabilized with FD: R_{32} (green triangles), R_{43} (pink diamonds), R_{21} (blue squares). Solid lines represent fits with the theoretical model, described in Section 2.2.1 and Ref. [15]. The permeability of the foams films, K_{foam}, is determined from the best fit of the data with the model. (For interpretation of the references to colour in this figure legend, the reader is referred to the web version of this article.)

flux across the adsorption layer. To check this explanation we performed additional series of experiments in which we extracted preformed bubbles from a sample of bulk foam, and then studied them in a "single bubble" experiment. These experiments showed that the gas permeability of the bubbles taken from bulk foams and of the "casual" single bubbles were almost the same, in the frame of our experimental accuracy. Thus we had to conclude that the adsorption layers in the experiments with single bubbles and with actual foams are rather similar and could not explain the differences shown in Fig. 8B.

Therefore, the most probable explanation for the different gas permeabilities, measured in actual foams and with single bubbles, is the non-equilibrium film thickness formed between ripening bubbles in bulk foams. Due to the high shear surface elasticity of the saponin adsorption layers, the time of foam film drainage, required to reach the equilibrium film thickness, was measured to be very long (more than 900 s) for saponin-stabilized foam films with diameter above 200 μm, whereas it is around 30 s for similar in diameter films, stabilized by low-molecular surfactants. Such slow film drainage takes place during foam coarsening and decreases significantly the rate of Ostwald ripening in the foams, due to the larger non-equilibrium foam film thickness. The latter effect is not important for the performed experiments with single bubbles, because the foam films in these experiments are much smaller in diameter (around 20 μm) and reach the equilibrium thickness within seconds, as confirmed by our microscopy observations.

It is worth emphasizing that, from the viewpoint of the quantitative characterization of the studied saponin systems, the experiments with single bubbles give more reliable results, as the data interpretation in these experiments is prompt to a minimal number of well-defined and justified assumptions.

3.5. *Effect of pH on Ostwald ripening in foams, stabilized with Escin and HC extract*

Within the obtained set of data, additional non-trivial information could be retrieved by comparing the results obtained with ES and HC extracts, because the HC extract contains 50 wt% of Escin as active saponin ingredient. Nevertheless, the experiments show that the foam films stabilized by HC extract have 4 times higher gas permeability, compared to the foams stabilized by pure ESC.

The significant difference between these two saponin systems could be attributed to several possible reasons: (1) The admixtures in the HC extract, which are not present in ESC, can interfere with the formation of the saponin adsorption layer and modify its major characteristics; (2) The different natural pH of the two saponin solutions (4.9 for HC, and 3.1 for Escin, see Table S1) can change the structure of the adsorption layer and the related gas permeability; (3) Different concentration of Ca^{2+} in the saponin extracts (0.17 mM in the solution of HC, and 0.034 mM in the solution of Escin) can affect the structure of the adsorption layers, because Ca^{2+} ions can form complexes with the hydroxyl groups of the sugar residues in the saponin molecules.

To clarify the relative importance of these effects, we studied the effects of pH and of Ca^{2+} concentration on the rate of bubble OR in foams. First, we performed a series of experiments with Escin and HC extracts, at pH varied in the range between 3 and 8. The pH was adjusted with solutions of HCl or NaOH and was verified to remain constant (within 0.05 units) during the entire duration of the experiments.

The results for K_{foam} as a function of pH, are shown in Fig. 9. The increase in pH leads to a noticeable increase of the gas permeability in foams stabilized by both HC and Escin. Qualitatively, K_{foam} follows the same dependence on pH for both saponins. However, K_{foam} is lower for Escin-stabilized foams in the entire range of pH values. These results clearly indicate that:

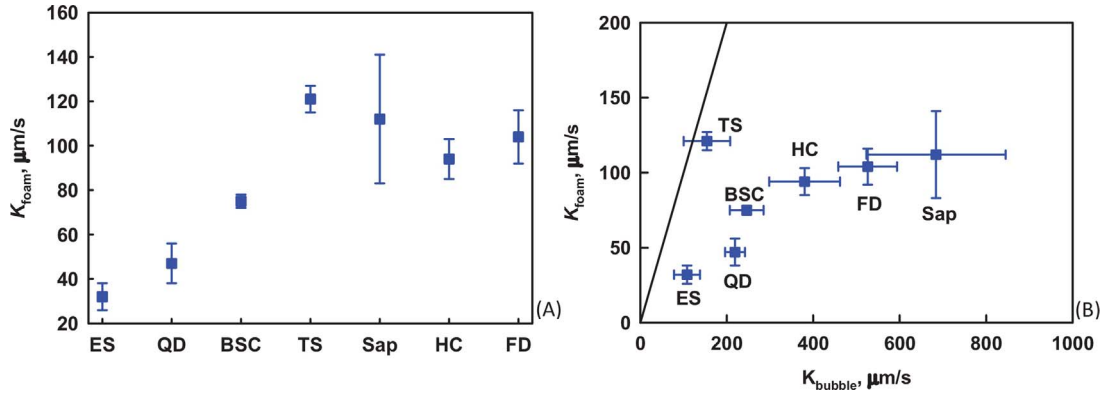

Fig. 8. (A) Gas permeability of foam films, stabilized by different saponin extracts, as determined from experiments with foams having air volume fraction of Φ = 90%; (B) Correlation between the gas permeability of the foam films, as determined from experiments with bulk foams, K_{foam}, and from experiments with single bubbles, K_{bubble} (the gas flux across the meniscus region is accounted for).

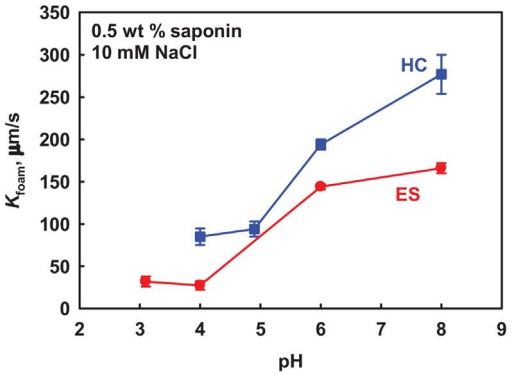

Fig. 9. Gas permeability as a function of the solution pH for foams stabilized by Escin (red circles) and HC (blue squares). (For interpretation of the references to colour in this figure legend, the reader is referred to the web version of this article.)

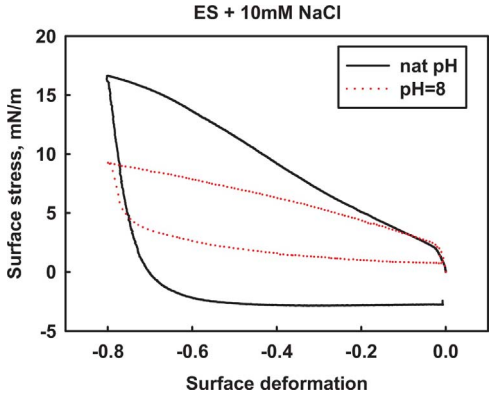

Fig. 10. Surface stress, as a function of the surface deformation, for Escin adsorption layers formed from solutions with natural pH = 3.1 and pH = 8.0. The experiments are performed with plate perpendicular to the barriers.

(1) The strong dependence of K_{foam} on pH should be related to changes in the structure of the adsorption layers, most probably caused by partial ionization of the COOH group in the Escin molecules at higher pH. Such ionization would hinder the formation of densely packed adsorption layer of saponin molecules, due to the electrostatic repulsion between the adsorbed molecules. Further indications for significant changes in the structure of the adsorption layer at high pH are presented in Fig. 10.
(2) The difference between the curves for Escin and HC shows that the presence of admixtures and/or Ca^{2+} ions in HC affects the properties of the adsorption layers and the rate of Ostwald ripening.
(3) The similarity in the shape of the two curves in Fig. 9 indicates that, still, Escin is the major surface active component in HC, while the admixtures and/or Ca^{2+} ions present in HC extract modify the adsorption layers which are dominated by Escin.

To confirm that the increase of pH changes the properties of Escin adsorption layers, we performed experiments with Escin adsorption layers, formed in Langmuir trough at different pH values. The obtained results from these experiments are compared in Fig. 10. One sees that the increase of pH from 3.1 to 8 decreases significantly the maximum surface stress for Escin adsorption layers, which is in a good agreement with the observed faster Ostwald ripening in the respective foams.

Similar set of experiments was performed at different concentrations of Ca^{2+} ions in the solutions, varied up to 2.5 mM. In contrast to the value of pH, the concentration of Ca^{2+} ions was found to have minor effect on the rate of Ostwald ripening and on the interfacial properties of the HC and ESC adsorption layers. We can conclude from these experiments that Escin is the dominant surface active component in HC extract (as expected). The main reasons for the observed differences between these two extracts are coming from (1) the different natural pH of the respective solutions (4.9 for HC and 3.1 for Escin), and (2) the presence of admixtures in the HC extract which are able to co-adsorb and to perturb the Escin molecular packing in the formed mixed adsorption layers.

4. Main results and conclusions

The main results from this study could be summarized as follows:

(1) New theoretical expression, accounting for the gas flux across the meniscus region of air bubble under air–solution interface, is derived and used to determine the gas permeability across the saponin adsorption layers, Eqs. (15) and (16). This expression should be used when the foam films are relatively small in diameter, as it is the case in the experiments with single bubbles having very small contact angles film-meniscus or in foams which are just above the close-packed volume fraction.
(2) The gas permeability across the adsorption layer correlates well with the surface stress, measured at very slow surface deformation (below 10^{-3} Hz) and does not correlate well with the surface elasticity, measured at faster surface deformation of 0.1 Hz. The comparison between the theoretically calculated rate of bubble diminishing and the respective experimental data clearly showed that the main gas transfer resistance arises from the saponin adsorption layers, formed on the foam film surfaces. Therefore, we can conclude that the main reason for the reduced rate of bubble Ostwald ripening in the saponin systems with high surface modulus is the low solubility and diffusivity of the gas molecules in the respective condensed adsorption layers (not the surface elasticity per se). The same conclusion was reached in our previous experiments with other surfactant systems with high surface elasticity [15]. Note that the latter conclusion cannot be applied to bubbles and foams stabilized by solid particle, where the particle adsorption could be truly irreversible and the process of Ostwald ripening could be entirely arrested due to jamming of the bubble surfaces.
(3) The gas permeability determined from the experiments with real foams, having air volume fraction of 90%, was significantly lower as compared to the gas permeability, determined from experiments with single bubbles. The performed experiments revealed that the latter effect is due to the much larger, non-equilibrium foam film thickness between neighboring bubbles in the actual foams, due to the very slow water drainage from the foam films with high surface shear and dilatational elasticity, stabilized by saponins.
(4) The adsorption layers of Escin at pH ≈ 3 have very low gas permeability (≈30 μm/s) and related very low rate of bubble Ostwald ripening in foams. On increase of pH up to 8, the Escin molecules become partially ionized, the respective adsorption layers become less densely packed, and their gas permeability increases up to ≈150 μm/s.

Supporting information

Table S1 contains information about studied saponins. Table S2 shows physico- chemical properties of studied saponin solutions. Table S3 presents the values for the gas permeability of foam films, formed between single bubbles and large air–water interface, and stabilized by different saponin solutions. Figure S1 presents the molecular structure of the saponins in the extracts studied. Figure S2 presents the method used for determination of the bubble size distribution and its evolution with time. Figure S3 presents the method of slow surface deformation in Langmuir trough. Figure S4 presents the evolution of the radius of single bubble under large air–water interface, in different saponin solutions. Figure S5 shows the dependence of the logarithm of the radius of a single bubble as function of the time. Figure S6 presents

schematically a bubble under a flat air–water interface. Figure S7 presents the gas permeability of the adsorption layers of various saponins, plotted versus the surface dilatational elasticity of the adsorption layers or versus the maximum surface stress.

Acknowledgments

The authors are grateful for the support to Unilever R & D Vlaardingen, and to COST Action MP1305. K.G. is grateful to the Marie Curie Intra-European fellowship program.

Appendix A. Supplementary data

Supplementary data associated with this article can be found, in the online version, at http://dx.doi.org/10.1016/j.colsurfa.2017.04.055.

References

[1] M.U. Vera, D.J. Durian, Enhanced drainage and coarsening in aqueous foams, Phys. Rev. Lett. 88 (2002) 088304/1–088304/4.
[2] S.J. Neethling, H.T. Lee, J.J. Cilliers, A foam drainage equation generalized for all liquid contents, J. Phys.: Condens. Matter 14 (2002) 331–342.
[3] A. Saint-Jalmes, Physical chemistry in foam drainage and coarsening, Soft Mater 2 (2006) 836–849.
[4] A. Saint-Jalmes, D. Langevin, Time evolution of aqueous foams: drainage and coarsening, J. Phys.: Condens. Matter 14 (2002) 9397–9412.
[5] H.M. Princen, The structure, mechanics, and rheology of concentrated emulsions and fluid foams, in: J. Sjöblom (Ed.), Encyclopedia of Emulsion Technology, Marcel Dekker, New York, 2001, p. 243 (chapter 11).
[6] D. Weaire, The rheology of foam, Curr. Opin. Colloid Interface Sci. 13 (2008) 171–176.
[7] D. Weaire, W. Drenckhan, Structure and dynamics of confined foams: a review of recent progress, Adv. Colloid Interface Sci. 137 (2008) 20–26.
[8] N.D. Denkov, S. Tcholakova, K. Golemanov, K.P. Ananthapadmanabhan, A. Lips, The role of surfactant type and bubble surface mobility in foam rheology, Soft Mater 5 (2009) 3389–3408.
[9] I. Lesov, S. Tcholakova, N. Denkov, Factors controlling the formation and stability of foams used as precursors of porous materials, J. Colloid Interface Sci. 426 (2014) 9–21.
[10] J.A. Attia, S. Kholi, L. Pilon, Scaling laws in steady-state aqueous foams including Ostwald ripening, Colloids Surf., A 436 (2014) 1000–1006.
[11] A.C. Martinez, E. Rio, G. Delon, A. Saint-Jalmes, D. Langevin, B.P. Binks, On the origin of the remarkable stability of aqueous foams stabilised by nanoparticles: link with microscopic surface properties, Soft Mater 4 (2008) 1531–1535.
[12] E. Rio, W. Drenckhan, A. Salonen, D. Langevin, Unusually stable liquid foams, Adv. Colloid Interface Sci. 205 (2014) 74–86.
[13] L.R. Arriaga, W. Drenckhan, A. Salonen, J.A. Rodrigues, R. Íñiguez- Palomares, E. Rio, D. Langevin, On the long-term stability of foams stabilised by mixtures of nano-particles and oppositely charged short chain surfactants, Soft Mater 8 (2012) 11085–11097.
[14] M. Abkarian, A.B. Subramaniam, S.-H. Kim, R.J. Larsen, S.-M. Yang, H.A. Stone, Dissolution arrest and stability of particle-covered bubbles, Phys. Rev. Lett. 99 (2007) 188301–188304.
[15] S. Tcholakova, Z. Mitrinova, K. Golemanov, N.D. Denkov, M. Vethamuthu, K.P. Ananthpadmanabhan, Control of bubble Ostwald ripening in foams by using surfactant mixtures, Langmuir 27 (2011) 14783–14796.
[16] T.B.J. Blijdenstein, P.W.N. de Groot, S.D. Stoyanov, On the link between foam coarsening and surface rheology: why hydrophobins are so different, Soft Mater 6 (2010) 1799–1808.
[17] A.J. Webster, M.E. Cates, Stabilization of emulsions by trapped species, Langmuir 14 (1998) 2068–2077.
[18] A.J. Webster, M.E. Cates, Osmotic stabilization of concentrated emulsions and foams, Langmuir 17 (2001) 595–608.
[19] K. Hostettmann, A. Marston, Saponins, Cambridge University Press, New York, 1995.
[20] J.-P. Vincken, L. Heng, A. De Groot, H. Gruppen, Saponins, classification and occurrence in the plant kingdom, Phytochemistry 68 (2007) 275–297.
[21] Q. Guglu-Ustundag, G. Mazza, Saponins: properties, applications and processing, Crit. Rev. Food Sci. Nutr. 47 (2007) 231–258.
[22] M. Piotrowski, J. Lewandowska, K. Wojciechowski, Biosurfactant-protein mixtures: Quillaja Bark Saponin at water/air and water/oil interfaces in presence of β-lactoglobulin, J. Phys. Chem. B 116 (2012) 4843–4850.
[23] K. Wojciechowski, Surface activity of saponin from Quillaja Bark at the air/water and oil/water interfaces, Colloids Surf. B 108 (2013) 95–102.
[24] K. Golemanov, S. Tcholakova, N.D. Denkov, E. Pelan, S.D. Stoyanov, Surface shear rheology of saponin adsorption layers, Langmuir 28 (2012) 12071–12084.
[25] K. Golemanov, S. Tcholakova, N.D. Denkov, E. Pelan, S.D. Stoyanov, Remarkably high surface visco-elasticity of adsorption layers of triterpenoid saponins, Soft Mater 9 (2013) 5738–5752.
[26] R. Stanimirova, K. Marinova, S. Tcholakova, N.D. Denkov, S. Stoyanov, E. Pelan, Surface rheology of saponin adsorption layers, Langmuir 27 (2011) 12486–12498.
[27] N. Pagureva, S. Tcholakova, K. Golemanov, N. Denkov, E. Pelan, S.D. Stoyanov, Surface properties of adsorption layers formed from triterpenoid and steroid saponins, Colloids Surf., A 491 (2016) 18–28.
[28] J. Milgate, D.C.K. Roberts, The nutritional and biological significance of saponins, Nutr. Res. 15 (1995) 1223–1249.
[29] S.G. Sparg, M.E. Light, J. van Staden, Biological activities and distribution of plant saponins, J. Ethnopharmacol. 94 (2004) 219–243.
[30] C.R. Sirtori, Aescin: pharmacology, pharmacokinetics, and therapeutic profile, Pharmacol. Res. 44 (2001) 183–193.
[31] M. Miyakoshi, Y. Tamura, H. Masuda, K. Mizutani, O. Tanaka, T. Ikeda, Antiyeast steroidal saponins from *Yucca schidigera* (Mohave Yucca), a new anti-food deteriorating agent, J. Nat. Prod. 63 (2000) 332–338.
[32] S. Piacente, C. Pizza, W. Oleszek, Saponins and phenolics of *Yucca schidigera* Roezl: Chemistry and bioactivity, Phytochem. Rev. 4 (2005) 177–190.
[33] D. Oakenfull, B.H. Arjmandi, Soy protein, saponins and plasma cholesterol, J. Nutr. 131 (2001) 2971–2972.
[34] S.-W. Kim, S.-K. Park, S.-I. Kang, H.-C. Kang, H.-J. Oh, C.-Y. Bae, D.-H. Bae, Hypocholesterolemic property of *Yucca schidigera* and *Quillaja saponaria* extracts in human body, Arch. Pharmacal Res. 26 (2003) 1042–1046.
[35] E. Ros, Intestinal absorption of triglycerides and cholesterol. Dietary and pharmacological inhibition to reduce cardiovascular risk, Artherosclerosis 151 (2000) 357–379.
[36] Food and Agriculture Organization, Quillaja extracts type 1 and 2: Chemical and Technical Assessment, 61st Report of the Joint FAO/WHO Expert Committee on Food Additives (JECFA), (2004).
[37] A. Scheludko, Thin liquid films, Adv. Colloid Interface Sci. 1 (1967) 391.
[38] N.D. Denkov, V. Subramanian, D. Gurovich, A. Lips, Wall slip and viscous dissipation in sheared foams: effect of surface mobility, Colloids Surf., A 263 (2005) 129–145.
[39] P.R. Garrett, J.D. Hines, S.C. Joyce, P.T. Whittal, Report prepared for Unilever R & D, Port Sunlight, 1993.
[40] Y. Wang, S.J. Neethling, The relationship between the surface and internal structure of dry foam, Colloids Surf., A 339 (2009) 73–81.
[41] R. Lemlich, Prediction of changes in bubble size distribution due to interbubble gas diffusion in foam, Ind. Eng. Chem. Fundam. 17 (1978) 89–93.
[42] H.M. Princen, S.G. Mason, The permeability of soap films to gases, J. Colloid Interface Sci. 20 (1965) 353–375.
[43] M. Nedyalkov, R. Krustev, D. Kashchiev, D. Platikanov, D. Exerowa, Permeability of Newtonian black foam films to gas, Colloid. Polym. Sci. 266 (1988) 291–296.
[44] R. Krustev, D. Platikanov, M. Nedyalkov, Permeability of common black foam films to gas. Part 1, Colloids Surf., A 79 (1993) 129–136.
[45] R. Krustev, D. Platikanov, M. Nedyalkov, Temperature dependence of gas permeability of Newton black films, Langmuir 12 (1996) 1688–1689.
[46] R. Krustev, D. Platikanov, M. Nedyalkov, Permeability of common black foamfilms to gas. Part 2, Colloids Surf., A 123–124 (1997) 383–390.
[47] P.A. Kralchevsky, K. Nagayama, Particles at Fluid Interfaces and Membranes: Attachment of Colloid Particles and Proteins to Interfaces and Formation of Two-Dimensional Arrays, Elsevier, Amsterdam, 2001.